metals

MDPI

Article

Optimizing Tempering Parameters to Enhance Precipitation Behavior and Impact Toughness in High-Nickel Steel

Guojin Sun [1,*] and Qi Wang [2]

[1] School of Engineering, Qinghai Institute of Technology, Xining 810016, China
[2] Electrical Engineering Division, Department of Engineering, University of Cambridge, Cambridge CB3 0FA, UK; qw273@cam.ac.uk
* Correspondence: guojinsun@qhit.edu.cn

Abstract: This study explores the effects of tempering on the precipitation behavior and impact toughness of high-nickel steel. The specimens underwent double quenching at 870 °C and 770 °C, followed by tempering at various temperatures. Advanced characterization techniques including optical microscopy (OM), scanning electron microscopy (SEM), and transmission electron microscopy (TEM) were used to elucidate precipitation phenomena. Additionally, electron backscatter diffraction (EBSD) was employed to assess the misorientation distribution after tempering. Charpy impact tests were performed on specimens tempered at different temperatures to evaluate their toughness. The findings reveal that with increasing tempering temperature, the fraction of low-angle grain boundaries decreases, which correlates positively with enhanced impact toughness. The results demonstrate that tempering at 580 °C optimizes the material's microstructure, achieving an impact toughness value of approximately 163 J.

Keywords: tempering process; precipitation; high-nickel steel; impact toughness; EBSD

check for updates

Citation: Sun, G.; Wang, Q. Optimizing Tempering Parameters to Enhance Precipitation Behavior and Impact Toughness in High-Nickel Steel. *Metals* **2024**, *14*, 898. https://doi.org/10.3390/met14080898

Academic Editor: Koh-ichi Sugimoto

Received: 13 July 2024
Revised: 2 August 2024
Accepted: 5 August 2024
Published: 7 August 2024

1. Introduction

In recent years, significant advancements have been made in understanding the role of nickel as an alloying element in steels. Nickel, particularly at concentrations around 4–5%, has been extensively studied for its effects on mechanical properties, including toughness, strength, and ductility. For instance, studies have shown that the addition of nickel enhances low-temperature toughness and resistance to brittle fracture, making it a crucial component in steels used for cryogenic applications [1,2]. Additionally, nickel's role in stabilizing austenite and suppressing martensitic transformations at lower temperatures has been well-documented, which is particularly beneficial in ensuring uniform mechanical properties across a range of service conditions [3,4].

Specifically, research by Kim et al. [5] demonstrated that a nickel content of approximately 4.5% significantly improves the impact toughness of medium-carbon steels, whilst maintaining a desirable balance with strength. This study aligns with other results [6], which highlighted the synergistic effects of nickel and other alloying elements, such as chromium and molybdenum, in enhancing corrosion resistance and mechanical robustness. Furthermore, recent EBSD-based analyses have provided new insights into the microstructural evolution during tempering, revealing complex interactions between precipitate formation and grain boundary characteristics [7,8]. For example, the work by Liesegang et al. [9] utilized EBSD to correlate grain boundary misorientation with mechanical performance, underscoring the importance of precise microstructural control.

Characterizing the misorientation between grains and within individual grains in metals is crucial, as it significantly influences mechanical properties across different temperatures, alongside physical, surface, and phase transformation properties. Misorientation analysis, particularly of grain boundaries and sub-grain structures, is now effectively

conducted using electron backscatter diffraction (EBSD). Understanding these aspects is vital for optimizing mechanical performance and tailoring material properties for specific applications [10–13]. By analyzing misorientation between lattices—expressed by rotation axes and angles—researchers can gain a comprehensive understanding of the roles of different phases in forming microstructures [14–16]. The ability to correlate misorientation data with mechanical properties makes EBSD an essential technique for developing advanced high-strength steels with improved performance characteristics.

Heat treatment is a critical method for enhancing the comprehensive mechanical properties of materials. In particular, the quenching and tempering processes are essential for improving the overall mechanical performance of nickel-alloy steels. The tempering process is especially significant as it involves the precipitation of phases, which greatly influences the mechanical properties of the material. Tempering involves heating the steel to a temperature below its critical point, followed by cooling, to achieve the desired mechanical properties through various transformation mechanisms. These mechanisms, which involve either long-range or short-range atomic transport, can be categorized into distinct stages based on microstructural evolution. The first stage of tempering (100–200 °C) involves the precipitation of ε-carbides. These carbides nucleate due to modulated structures formed during low-temperature aging, and at the end of this stage, martensite retains its tetragonality. In low-carbon steels, this stage may not be prominent due to limited ε-carbide formation [17]. The second stage (200–300 °C) is characterized by the decomposition of residual austenite into ferrite and cementite, driven by carbon diffusion in the austenite. During the third stage (200–350 °C), cementite appears with a Widmanstätten distribution, characterized by a specific orientation relationship with the matrix. In the fourth stage (400–700 °C), cementite particles coarsen and lose their crystallographic morphology, and martensite lath boundaries are replaced by equiaxed ferrite grain boundaries [18–22]. By optimizing the tempering parameters, the microstructure and mechanical properties of high-nickel steel can be tailored to meet specific industrial requirements.

Despite these advancements, there remains a lack of comprehensive studies focusing on the optimization of tempering parameters specifically for high-nickel steels, especially those with a 4.5% nickel content. This study addresses this gap by investigating the effects of different tempering temperatures on the microstructure and mechanical properties of such steels. By leveraging advanced characterization techniques, including SEM, TEM, and EBSD, this research aims to provide a detailed understanding of the microstructural mechanisms at play and their implications for industrial applications.

2. Experimental Procedures and Sample Characterization

In this study, high-nickel alloy steel samples were prepared with a chemical composition, as specified in Table 1. The steel plates were initially machined into cuboid specimens with dimensions of 150 mm × 80 mm × 20 mm. Prior to heat treatment, all samples were polished to remove surface oxides and then subjected to double quenching at 870 °C and 770 °C for 1 h. After quenching, the samples underwent tempering at various temperatures (500 °C, 580 °C, and 620 °C) for 2 h. The phase transformation temperatures of the material were measured using dilatometry (NETZSCH DIL 402 C, Hanau, Germany). As shown in Figure 1, the Ac1 and Ac3 temperatures were determined to be 692.1 °C and 786.8 °C, respectively.

Table 1. Chemical composition of the high-nickel alloy steel (wt.%).

Element	C	Si	Ni	P	Si	S	Mn	Cr	Cu	V	Mo
Content	0.1	0.2	4.5	0.01	0.25	0.01	0.5	1.5	0.2	0.06	0.5

After heat treatment, V-notch Charpy impact specimens with dimensions of 10 mm × 10 mm × 55 mm (as shown in Figure 2) were machined from the steel plates. The Charpy impact tests were conducted at −20 °C to evaluate the impact toughness of the specimens.

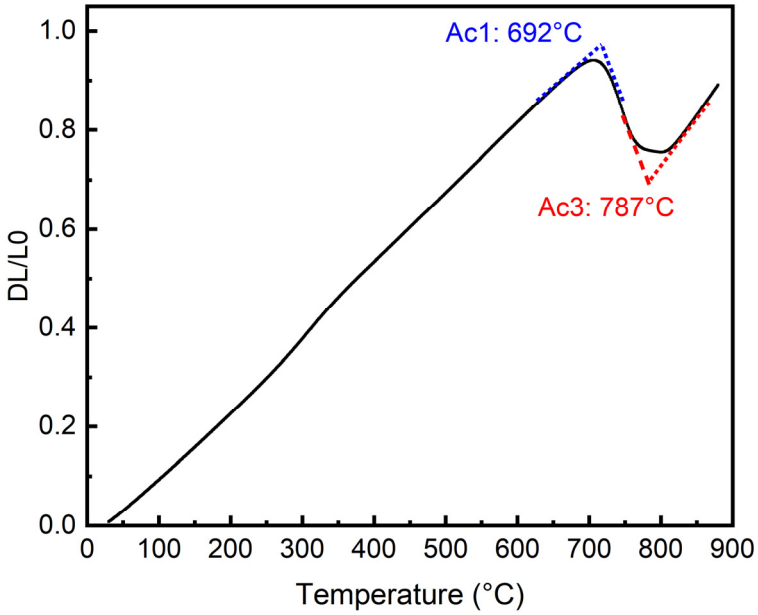

Figure 1. Dilatometry measurement of phase transformation temperatures.

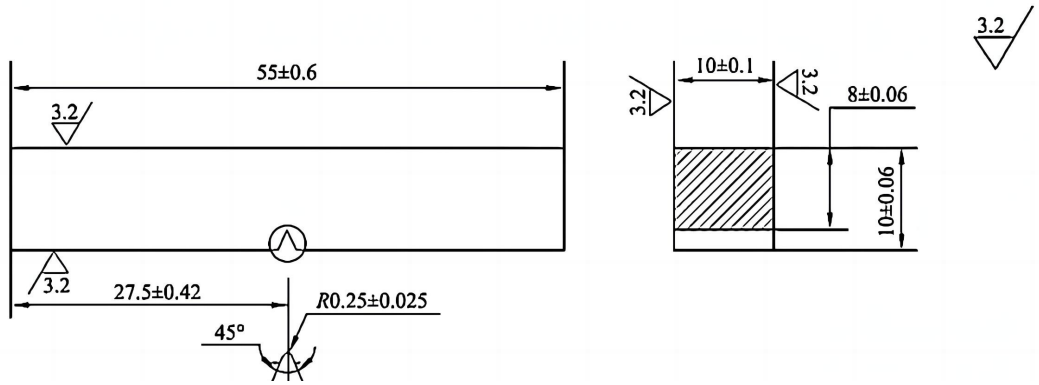

Figure 2. Standard Charpy impact specimen (unit: mm).

For microstructural characterization, the samples were mechanically polished and etched using a 4% Nital solution. Optical microscopy (OM) was employed to observe the general microstructure. Scanning Electron Microscopy (SEM) analysis was conducted using a JEOL JSM-7800F microscope (Akishima, Japan), which offers high-resolution imaging and elemental analysis capabilities. The accelerating voltage was set at 15 kV, and secondary electron imaging was utilized to observe surface features. Electron Backscatter Diffraction (EBSD) was conducted on a field emission gun scanning electron microscope equipped with an Oxford Instruments HKL EBSD system. The EBSD data were analyzed to determine the crystallographic orientations and misorientation distributions. The samples were prepared for EBSD analysis by electropolishing to remove surface artifacts and achieve a clean and flat surface. Transmission Electron Microscopy (TEM) was performed using a JEOL JEM-2100 microscope (Akishima, Japan), operating at an accelerating voltage of 200 kV. The samples for TEM analysis were prepared using mechanical thinning followed by ion milling to obtain electron-transparent specimens.

3. Results and Discussion

Tempering at temperatures below the Ac1 temperature is a critical step in heat treatment, affecting the redistribution or precipitation of carbon and alloying elements as carbides depending on the tempering temperature, which in turn enhances the mechanical properties of steels. During tempering, the dislocation density decreases, and residual

stresses from quenching are relieved. This section presents the detailed results of the microstructural and mechanical property analyses performed on the high-nickel steel after tempering at various temperatures. Figure 1 shows the SEM microstructures at various tempering temperatures.

After tempering for 2 h, fine carbides precipitate, as observed in Figure 3b–d for tempering temperatures of 500 °C, 580 °C, and 620 °C, respectively. At 500 °C, the microstructure shows a significant number of fine carbides distributed within the martensitic matrix, predominantly precipitating along the lath boundaries and within the laths. This distribution is critical in enhancing the steel's hardness and wear resistance. Cementite particles precipitate within the martensite and along lath orientations, contributing to the overall hardness and stability of the microstructure [23–25].

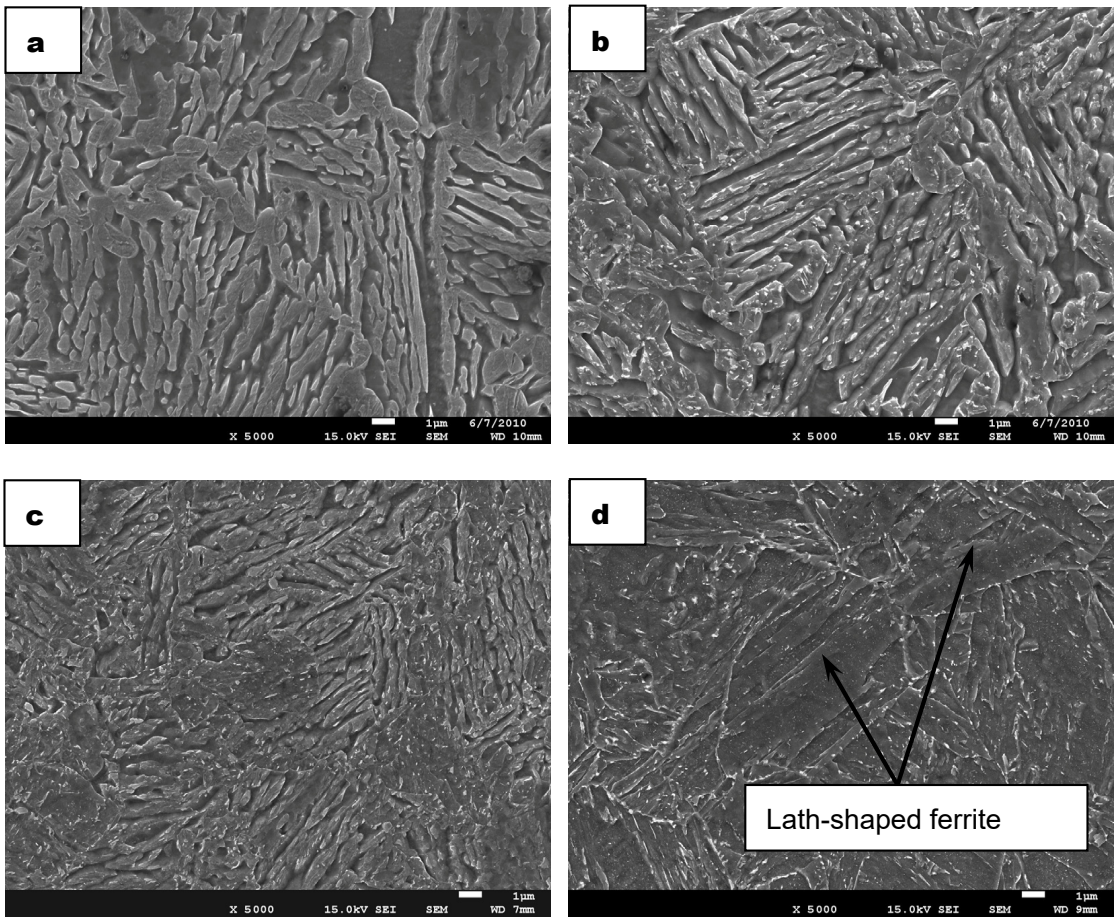

Figure 3. SEM images of steel at various tempering temperatures for 2h. (**a**) As-quenched; (**b**) 500 °C; (**c**) 580 °C; (**d**) 620 °C.

The addition of alloying elements, such as nickel and molybdenum, significantly affects the precipitation behavior during tempering. These elements play a crucial role in stabilizing the carbides and preventing their coarsening. Notably, tempering at 580 °C results in fine precipitates without significant coarsening, attributable to the segregation of alloying elements at the carbide–ferrite interface. This segregation acts as a barrier to carbon diffusion, thereby maintaining the fine precipitate size and ensuring a uniform distribution throughout the matrix. The presence of alloying elements in the cementite structure inhibits its coarsening during the fourth stage of tempering. This inhibition is particularly beneficial as it helps maintain the mechanical properties of the steel, such as toughness and hardness, over extended periods [26].

Although martensite lath boundaries remain stable up to approximately 620 °C, considerable dislocation rearrangement occurs within the laths. This rearrangement leads

to the formation of lath-shaped ferrite grains derived from martensite, as indicated in Figure 3d. At 620 °C, the microstructure undergoes more pronounced changes. The precipitates begin to coarsen significantly, and the martensitic laths transform into equiaxed ferrite grains. This transformation is accompanied by a decrease in hardness and an increase in toughness, as the steel's microstructure becomes more stable and less prone to brittle fracture.

Figure 4 presents the misorientation distributions after tempering at 500 °C, 580 °C, and 620 °C. And Figure 5 displays the misorientation angles within a single grain.

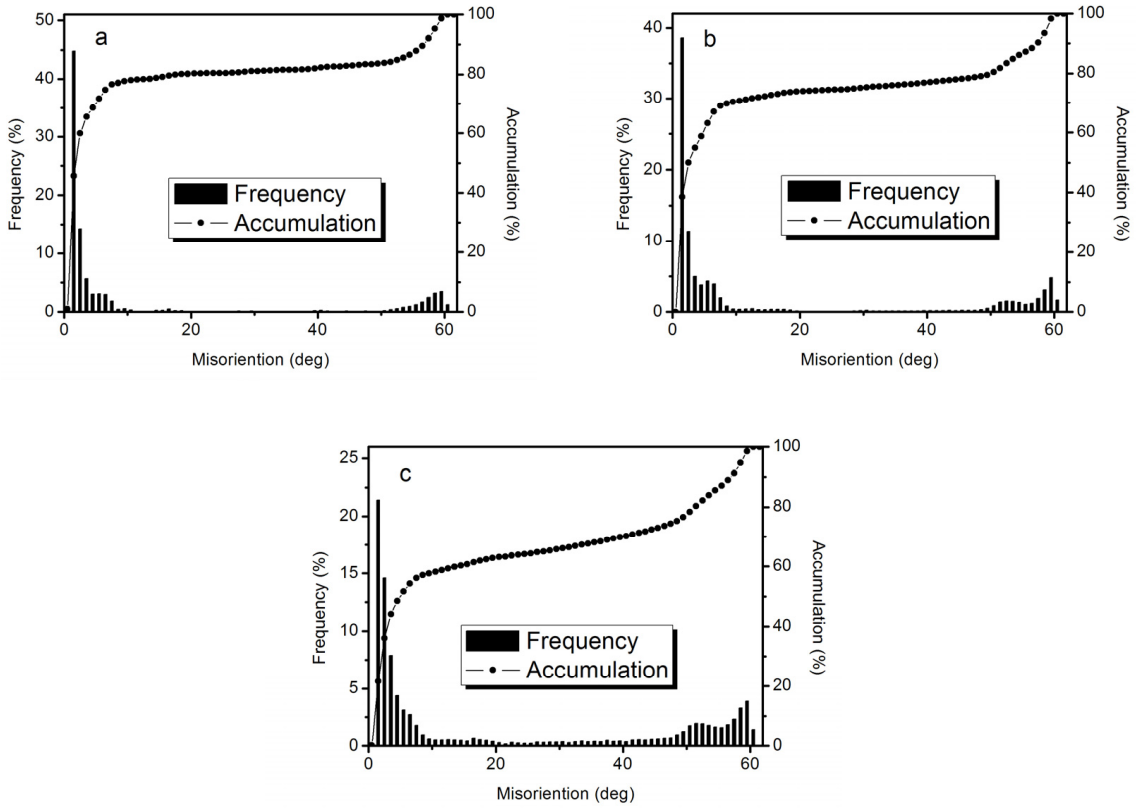

Figure 4. Misorientation distribution at different tempering temperatures. (**a**) 500 °C; (**b**) 580 °C; (**c**) 620 °C.

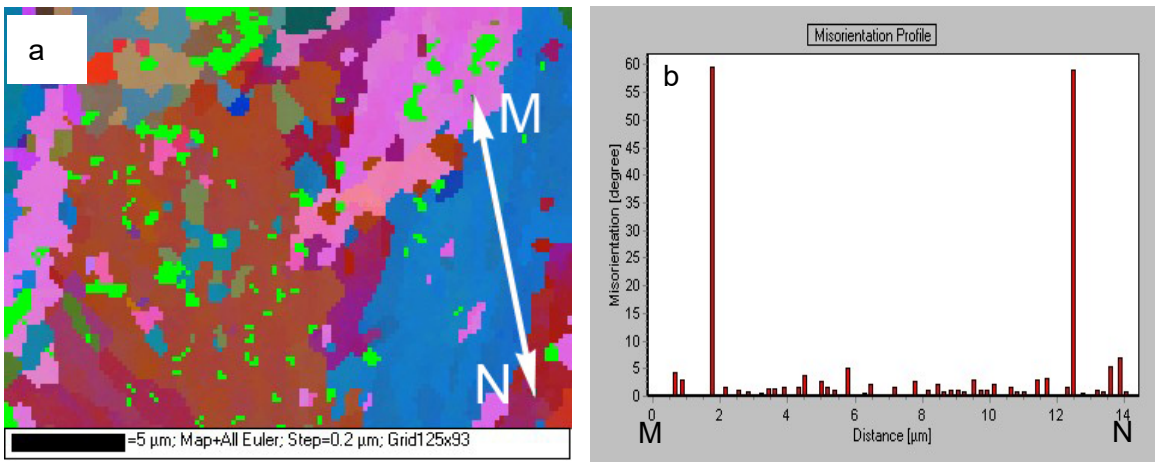

Figure 5. *Cont.*

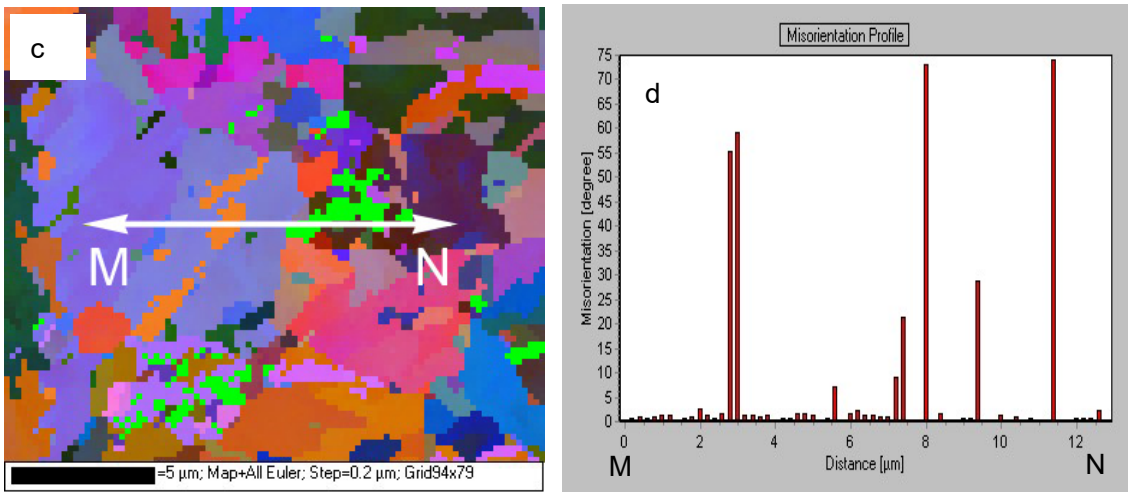

Figure 5. Misorientation distribution within grains at different tempering temperatures (**a**,**b**) at 500 °C and (**c**,**d**) at 620 °C.

At 500 °C, low-angle boundaries (angles less than 10°) exceed 75%, indicating a high density of dislocations and sub-grain boundaries, which contribute to the material's strength but also to its brittleness, as shown in Figure 4a. At 580 °C, low-angle boundaries decrease to about 70%, indicating that precipitation particles lose their orientations. This reduction in low-angle boundaries is beneficial, as it leads to a more random distribution of precipitates, which enhances the mechanical properties, particularly impact toughness. The random distribution helps to interrupt crack propagation pathways, thereby increasing the material's ability to absorb impact energy. At 620 °C, low-angle boundaries further decrease, as shown in Figure 4c, leading to coarsened precipitates as finer particles dissolve into the matrix to support the growth of larger particles.

This coarsening effect is significant as it indicates the movement and redistribution of alloying elements within the microstructure, which impacts the overall toughness and ductility of the steel. Figure 5a,b show that at 500 °C, misorientation angles within a grain do not exceed 5°, suggesting a relatively uniform strain distribution within the grains. However, at 620 °C, misorientation angles range from 5° to 12°, as shown in Figure 5c,d, suggesting a more heterogeneous strain distribution. The presence of misorientation angles at these specific values suggests the formation of a mixed grain boundary character, including both low-angle grain boundaries (LAGBs) and high-angle grain boundaries (HAGBs). The histogram clearly demonstrates an increased frequency of higher misorientation angles, correlating with the advanced stage of carbide coarsening. These higher misorientation angles absorb less energy and provide minimal resistance to crack propagation, which can lead to reduced toughness. This indicates that, while tempering at higher temperatures can reduce residual stresses and dislocation densities, it can also introduce larger grain boundary misorientations that might detract from the material's overall toughness and impact resistance.

The evolution of precipitation with increasing tempering temperature is shown in Figure 6.

From Figure 6 it can be seen that the number of precipitates decreases slightly as the tempering temperature rises. At 500 °C, precipitates typically follow a Widmanstätten distribution, characterized by a specific crystallographic orientation. By 580 °C, precipitates lose their distinct crystallographic morphology due to reduced dislocations and the onset of spheroidization, where smaller precipitates begin to dissolve into the matrix. This dissolution provides carbon and alloying elements for the selective growth of larger particles. At 620 °C, this phenomenon becomes more pronounced. The increased temperature accelerates the diffusion rates of carbon and alloying elements, leading to significant coarsening of precipitates. Smaller particles dissolve, contributing to the growth of larger precipitates,

which now dominate the microstructure. This coarsening results in a more homogeneous distribution throughout the matrix, which can influence the steel's mechanical properties. The changes in precipitate size and distribution are crucial for understanding the impact of tempering temperature on the material's performance, particularly its impact toughness and strength [27].

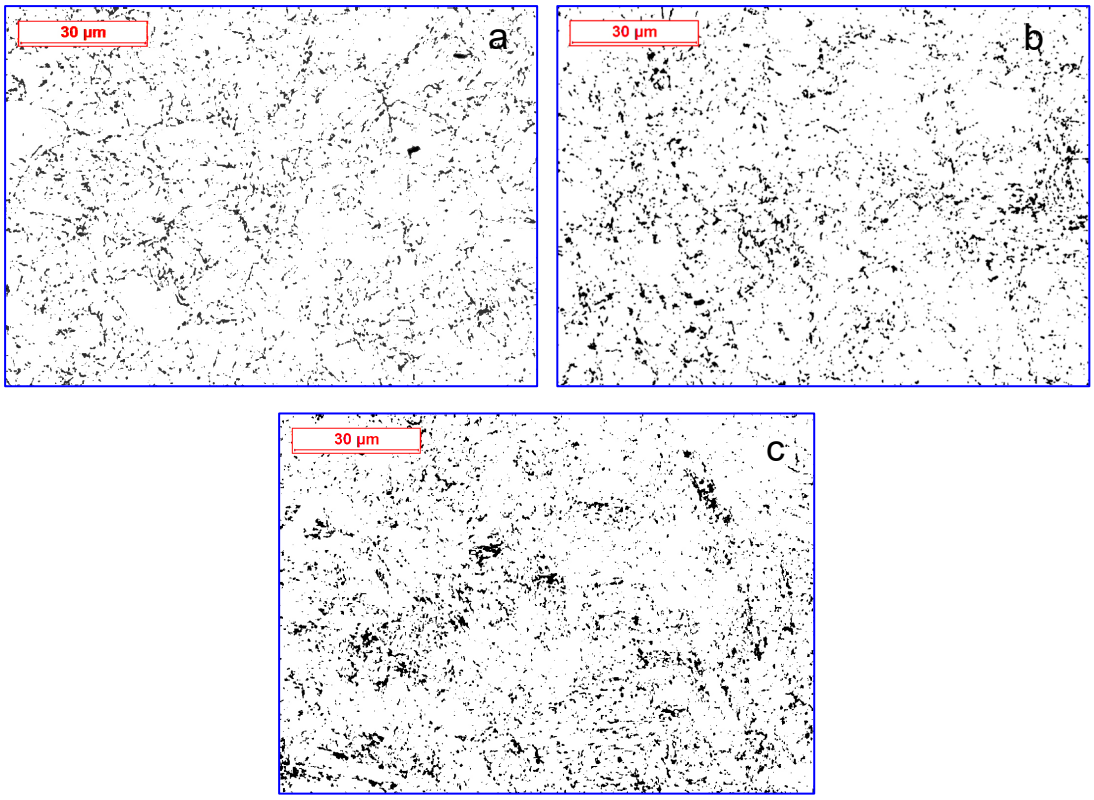

Figure 6. Precipitation distribution at various tempering temperatures: (**a**) 500 °C; (**b**) 580 °C; (**c**) 620 °C.

TEM images of steel after tempering are shown in Figure 7, offering more detailed insights than SEM and OM. The precipitation size distributions as a function of tempering temperature were also counted, which are shown in Figure 8.

In the TEM images, fine carbides were observed and their morphology, size, and distribution were analyzed. Figure 7a–c correspond to the samples tempered at 500 °C, 580 °C, and 620 °C, respectively. The precipitates were highlighted in these images by marking them with circles for clarity and easy identification.

From the results of Figures 7 and 8, it can been seen that fine carbides precipitate during tempering, significantly influenced by temperature. At the tempering temperature of 580 °C, the precipitates are fine and uniformly distributed, predominantly along specific orientations within the martensitic structure [28]. These carbides are small, typically less than 20 nm in diameter. At a tempering temperature of 580 °C, the precipitates become slightly larger and more widely distributed. The carbides at this stage begin to lose their preferential orientation, indicating the onset of spheroidization. The observed carbides range from 20 to 25 nm in size without significant coarsening (Figure 8b). However, at 620 °C, there is notable coarsening of the precipitates, with many carbides exceeding 25 nm. The microstructure reveals a more pronounced dissolution of smaller precipitates into the matrix and the growth of larger particles, indicating advanced coarsening processes, as evidenced by a second peak in the distribution curve (Figure 8c).

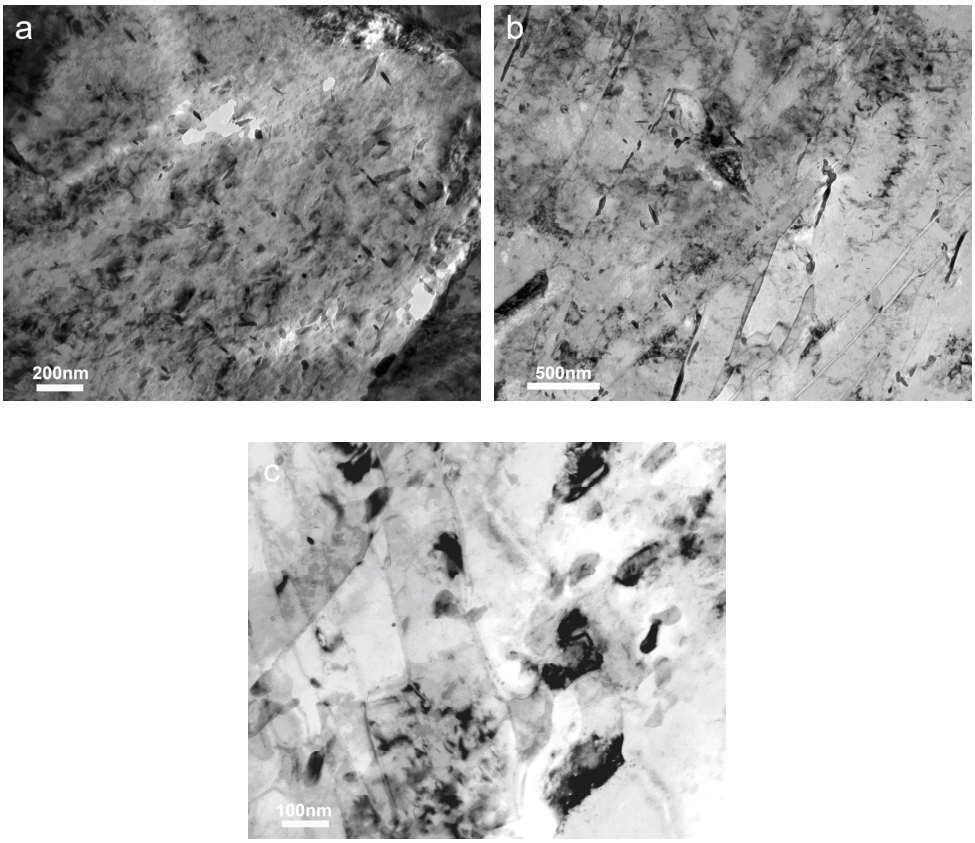

Figure 7. TEM images of steel at various tempering temperatures: (**a**) 500 °C; (**b**) 580 °C; (**c**) 620 °C.

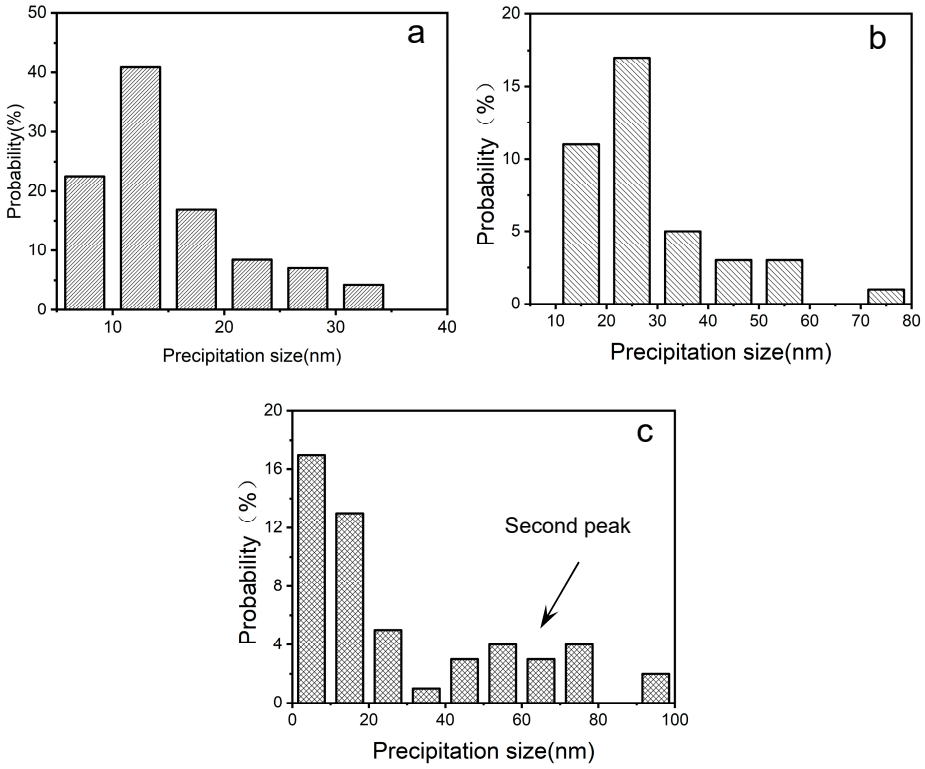

Figure 8. Precipitation size distribution curves at different tempering temperatures: (**a**) 500 °C; (**b**) 580 °C; (**c**) 620 °C.

To thoroughly understand the microstructural evolution and mechanical properties of the high-nickel steel, it is essential to determine the phase composition of the precipitates. Energy-dispersive X-ray spectroscopy (EDX), combined with transmission electron microscopy (TEM), was used to analyze the chemical composition of the precipitates and infer their phase nature. The analysis results for the precipitates and matrix at 620 °C are shown in Figure 9. The EDX spectrum of the matrix reveals distinct peaks for Ni, Fe, and C elements. In contrast, the EDX spectrum of the precipitates shows a prominent peak for Cr, indicating that the precipitates are Cr-based alloy precipitates. Based on the tempering temperatures used in this study and comparisons with other research, the precipitates are tentatively identified as M7C3 carbides. The formation of these complex carbides is attributed to the segregation of alloying elements at the carbide–matrix interface, a phenomenon that becomes more pronounced at elevated temperatures [28].

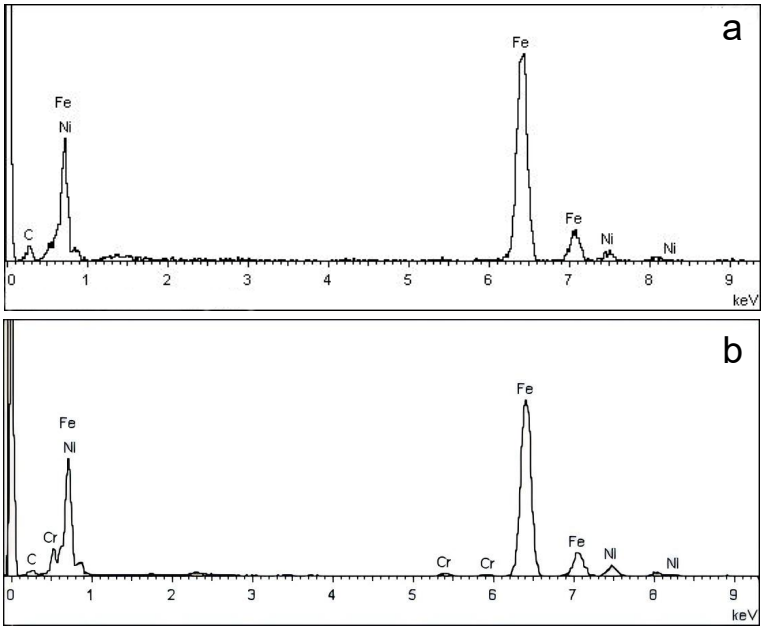

Figure 9. EDX results for the matrix and precipitates: (**a**) matrix; (**b**) precipitates.

This redistribution and growth of carbides play a critical role in the resulting mechanical properties of the steel, such as impact toughness. Furthermore, the detailed TEM analysis underscores the complex interplay between tempering temperature and carbide evolution, emphasizing the necessity of precise temperature control during heat treatment to achieve the desired mechanical properties. The influence of tempering temperature on the impact toughness of steel is shown in Figure 10.

The impact toughness curve in Figure 10 reflects the evolution of carbides with increasing tempering temperature. At 500 °C, there is significant variability in impact toughness values. This is attributed to the orientation of the fine precipitates, as shown in Figure 3b, and the prevalence of low-angle boundaries, as depicted in Figures 4a and 5b. The orientation of fine precipitates and the high density of low-angle boundaries contribute to the moderate impact toughness observed at this temperature.

At 580 °C, the orientation of carbides decreases (Figure 3c), and the proportion of low-angle boundaries also diminishes (Figure 4b), resulting in a peak in impact toughness, with an average value reaching 163 J. This improvement is due to the more random distribution of precipitates and the enhanced dislocation mobility, which reduces variability in impact toughness values and indicates more consistent mechanical properties. However, at 620 °C, impact toughness begins to decline, and the variability in values increases. This is due to the coarsening of carbides (Figure 8c), where larger, coarsened carbides become less effective at impeding crack propagation, leading to reduced impact toughness. Additionally, the

increase in high-angle boundaries at this temperature decreases the material's ability to absorb impact energy, further contributing to the reduction in toughness.

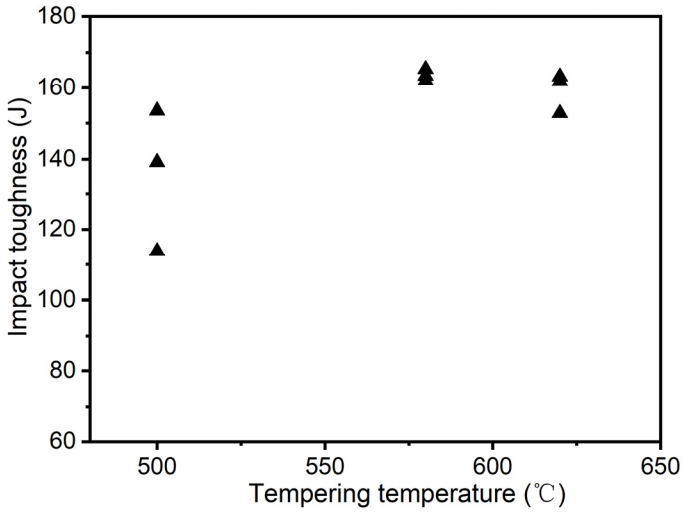

Figure 10. Impact toughness after tempering.

4. Conclusions

This study comprehensively investigates the influence of tempering temperature on the precipitation behavior, misorientation distribution, and impact toughness of high-nickel steel. The following key conclusions can be drawn:

(1) Tempering high-nickel steel at different temperatures significantly influences the precipitation of carbides. At 500 °C, the steel exhibits a prevalence of fine carbides. As the tempering temperature is raised to 580 °C, the carbides start to lose their distinct crystallographic morphology. By 620 °C, substantial coarsening of the carbides is observed, with smaller precipitates dissolving and larger particles growing.

(2) The study indicates that the proportion of low-angle grain boundaries decreases with increasing tempering temperature. At 500 °C, low-angle boundaries constitute over 75% of the grain boundaries. This proportion decreases to about 70% at 580 °C and further declines at 620 °C. The reduction in low-angle boundaries is associated with the randomization of precipitate orientations, which enhances the steel's impact toughness up to 580 °C. However, at 620 °C, the formation of high-angle boundaries and the coarsening of carbides adversely affect the toughness.

(3) The impact toughness of the steel improves with increasing tempering temperature, peaking at 163 J at 580 °C. This peak corresponds to an optimal balance of fine, randomly distributed precipitates. Beyond this temperature, specifically at 620 °C, the coarsening of carbides and the rise in high-angle grain boundaries result in a reduction in impact toughness. These findings highlight the critical importance of precise temperature control during tempering to achieve the desired mechanical properties in high-nickel steels.

Author Contributions: Conceptualization, G.S.; methodology, G.S.; investigation, G.S.; software, Q.W.; data curation, Q.W. All authors have read and agreed to the published version of the manuscript.

Funding: The authors acknowledge financial support from the Kunlun Talent Project of Qinghai Province (2023-QLGKLYCZX-032).

Data Availability Statement: The data presented in this study are available on request from the corresponding author due to privacy.

Conflicts of Interest: The authors declare that they have no known competing financial interests or personal relationships that could have appeared to influence the work reported in this paper.

References

1. Zhang, W.X.; Chen, Y.Z.; Cong, Y.B.; Liu, Y.H.; Liu, F. On the austenite stability of cryogenic Ni steels: Microstructural effects: A review. *J. Mater. Sci.* **2021**, *56*, 12539–12558. [CrossRef]
2. Xiong, T.; Xu, G.; Yuan, Q.; Hu, H.-J.; Tian, J.-Y. Effects of initial austenite grain size on microstructure and mechanical properties of 5% nickel cryogenic steel. *Met. Microstruct. Anal.* **2019**, *8*, 241–248. [CrossRef]
3. Wu, S.; Sun, G.; Ma, Q.; Shen, Q.; Xu, L. Influence of QLT treatment on microstructure and mechanical properties of a high nickel steel. *J. Mech. Work. Technol.* **2013**, *213*, 120–128. [CrossRef]
4. Nakanishi, D.; Kawabata, T.; Aihara, S. Effect of dispersed retained γ-Fe on brittle crack arrest toughness in 9% Ni steel in cryogenic temperatures. *Mater. Sci. Eng. A* **2018**, *723*, 238–246. [CrossRef]
5. Kim, J.I.; Kim, H.J.; Morris, J.W. The role of the constituent phases in determining the low temperature toughness of 5.5Ni cryogenic steel. *Met. Trans. A* **1984**, *15*, 2213–2219. [CrossRef]
6. Zhao, X.-Q.; Pan, T.; Wang, Q.-F.; Su, H.; Yang, C.-F.; Yang, Q.-X. Effect of tempering temperature on microstructure and mechanical properties of steel containing Ni of 9%. *J. Iron Steel Res. Int.* **2011**, *18*, 47–51. [CrossRef]
7. Cui, X.-B.; Liu, T.-L.; Zheng, Z.-B.; Guo, Z.-Q.; Zheng, K.-H.; Han, P.-X. Effects of Ni content and tempering temperatures on microstructure and properties of medium-carbon cast steel. *J. Iron Steel Res. Int.* **2023**, *30*, 1524–1536. [CrossRef]
8. Zhao, F.; Zhang, S.; Cheng, T.; Su, L.; Zhang, Z. Ultrastrong Low-Alloy Steel with Good Ductility via Multiple Strengthening, Suppressed Carbides and Reversed Austenite in Quenching and Tempering. *Met. Mater. Trans. A* **2024**, *55*, 2400–2413. [CrossRef]
9. Liesegang, M.; Lion, P.; Beck, T.; Gräf, M.; Steidl, G. Investigation of the tensile deformation behaviour in Ni-based superalloy inconel alloy 617 using EBSD-based finite element simulations and optical flow method. *J. Mater. Sci.* **2023**, *58*, 8990–9005. [CrossRef]
10. Dobe, R.; Das, A.; Mukherjee, R.; Gupta, S. Evaluation of grain boundaries as percolation pathways in quartz-rich continental crust using Atomic Force Microscopy. *Sci. Rep.* **2021**, *11*, 9831. [CrossRef]
11. Dey, S.; Chatterjee, S.; Ritanjali, S.R.; Dobe, R.; Mukherjee, R.; Mandal, S.; Gupta, S. Nanoscale visualization of high-angle misorientations in quartz-rich rocks using SEM-EBSD and Atomic Force Microscopy. *J. Struct. Geol.* **2024**, *183*, 105146. [CrossRef]
12. Jiang, R.; Zhang, W.; Zhang, L.; Zhao, Y.; Zhang, L.; Song, Y. Strain localization and crack initiation behavior of a PM Ni-based superalloy: SEM-DIC characterization and crystal plasticity simulation. *Fatigue Fract. Eng. Mater. Struct.* **2022**, *45*, 1635–1651. [CrossRef]
13. Li, C.; Dubovi, J.; Klein, C. Application of electron backscatter diffraction in facet crystalline orientation study of Al-Cu-Fe alloy. *Mater. Charact.* **2022**, *191*, 112158. [CrossRef]
14. Xu, J.; Brodin, H.; Peng, R.L.; Luzin, V.; Moverare, J. Effect of heat treatment temperature on the microstructural evolution of CM247LC superalloy by laser powder bed fusion. *Mater. Charact.* **2022**, *185*, 111742. [CrossRef]
15. Liang, G.; Tan, Q.; Liu, Y.; Schneider, M.; Detemple, E.; Eggeler, G. Effect of cooling rate on microstructure and mechanical properties of a low-carbon low-alloy steel. *J. Mater. Sci.* **2021**, *56*, 3995–4005. [CrossRef]
16. Yaso, M.; Hayashi, S.; Morito, S.; Takuya, O.; Kunichika, K.; Kouji, M. Characteristics of Retained Austenite in Quenched High Carbon-High Chromium Alloy Steels. *J. Jpn. Inst. Met.* **2009**, *73*, 852–856. [CrossRef]
17. Kawahara, Y.; Kaneko, K.; Sawada, H.; Takahashi, J. Transition from carbon clusters to ε, θ-carbides in a quenched and aged low-carbon ferritic steel. *Acta Mater.* **2023**, *252*, 118919. [CrossRef]
18. Zeng, T.Y.; Li, W.; Wang, N.M.; Wang, W.; Yang, K. Microstructural evolution during tempering and intrinsic strengthening mechanisms in a low carbon martensitic stainless bearing steel. *Mater. Sci. Eng. A* **2022**, *836*, 142736. [CrossRef]
19. Farber, V.M.; Khotinov, V.A.; Selivanova, O.V.; Ovsyannikov, A.B.; Karabanalov, M.S. Evolution of the Structure and Mechanical Properties of Medium-Carbon Microalloyed Steel during High-Temperature Tempering. *Phys. Met. Metallogr.* **2023**, *124*, 824–830. [CrossRef]
20. Hu, J.; Liu, Y.; Wang, G.; Li, Q.; Wen, J.; Yan, L.; Chen, S.; Gu, Y. Effect of Tempering Treatment on Microstructural Evolution and Mechanical Behavior of Heavy-Wall Heat Induction Seamless Bend Pipe. *Materials* **2022**, *15*, 259. [CrossRef]
21. Liu, J.; Wei, S.; Sun, J.; Lu, S. Effect of Tempering Temperature on the Microstructural Evolution and Properties of 800 MPa Grade Low-Carbon Bainite-Deposited Metals. *Metall. Mater. Trans. A Phys. Metall. Mater. Sci.* **2022**, *53*, 4272–4282. [CrossRef]
22. He, B.B.; Guan, Q.W. Effect of Ausforming Strain on the Microstructural Evolution of Lath Martensite in Low Carbon Steel. *Met. Mater. Int.* **2022**, *28*, 2330–2339. [CrossRef]
23. Chakraborty, A.; Webster, R.F.; Primig, S. Lath martensite substructure evolution in low-carbon microalloyed steels. *J. Mater. Sci.* **2022**, *57*, 10359–10378. [CrossRef]
24. Wang, E.; Ding, C.; Gong, N.; Gu, C.; Liu, H.; Li, L.; Wu, H.; Niu, G. Effect of Nb Precipitates and Reversed Austenite Formed by QLT Process on Microstructure and Mechanical Properties of Nb-Bearing 7Ni Cryogenic Steel. *Met. Mater. Trans. A* **2024**, *55*, 247–260. [CrossRef]
25. Masoumi, M.; Centeno, D.M.A.; Tressia, G.; Correa, P.A.; Ariza, E.A.; Mola, J. Microstructural Design via Quenching and Partitioning for Enhanced Mechanical and Wear Properties in AISI 9254 Spring Steel: A Comprehensive Investigation. *Met. Mater. Trans. A* **2024**, *55*, 3364–3387. [CrossRef]
26. Liang, J.X.; Wang, Y.C.; Cheng, X.W.; Li, Z.; Du, J.K.; Li, S.K. Microstructure and mechanical properties of a Cr–Ni–W–Mo steel processed by thermo-mechanical controlled processing. *J. Iron Steel Res. Int.* **2021**, *28*, 713–721. [CrossRef]

27. Zhu, Y.; Zhang, Q.; Yuan, Q.; Guan, J.; Yang, Y.; Xu, G. Effects of Tempering Temperature on the Microstructure, Strength, and Toughness of Medium-Carbon Ti–Mo-Bearing Martensitic Steel. *Arab. J. Sci. Eng.* **2022**, *47*, 9061–9073. [CrossRef]
28. Fan, Z.J.; Shen, Y.Z.; Xu, Z.Q.; Zhu, P.C.; Liu, H.; Ma, Y.F.; Guan, W.Q. Evolution of Precipitate Phases in Ferritic and Martensitic Steel P92 During Normalizing and Tempering. *JOM* **2022**, *74*, 3578–3594. [CrossRef]